1-2021

Monitoring Tropical Forest Succession at Landscape Scales Despite Uncertainty in Landsat Time Series

T. Trevor Caughlin
Boise State University

Cristina Barber
Boise State University

Gregory P. Asner
Arizona State University

Nancy F. Glenn
Boise State University

Stephanie A. Bohlaman
University of Florida

See next page for additional authors

Ecological Applications, 31(1), 2021, e02208

Monitoring tropical forest succession at landscape scales despite uncertainty in Landsat time series

T. Trevor Caughlin [1,8], Cristina Barber [1], Gregory P. Asner [2,3], Nancy F. Glenn [4,5], Stephanie A. Bohlman [6], and Chris H. Wilson [7]

[1]*Biological Sciences, Boise State University, Boise, Idaho 83725 USA*
[2]*Center for Global Discovery and Conservation Science, Arizona State University, Hilo, Hawaii 96720 USA*
[3]*Center for Global Discovery and Conservation Science, Arizona State University, Tempe, Arizona 85287 USA*
[4]*Department of Geosciences, Boise State University, Boise, Idaho 83725 USA*
[5]*School of Civil and Environmental Engineering, University of New South Wales, Sydney 2052 Australia*
[6]*School of Forest Resources and Conservation, University of Florida, Gainesville, Florida 32611 USA*
[7]*Agronomy Department, University of Florida, Gainesville, Florida 32611 USA*

Citation: Caughlin, T. T., C. Barber Alvarez-Buylla, G. P. Asner, N. F. Glenn, S. A. Bohlman, and C. H. Wilson. 2021. Monitoring tropical forest succession at landscape scales despite uncertainty in Landsat time series. Ecological Applications 31(1):e02208. 10.1002/eap.2208

Abstract. Forecasting rates of forest succession at landscape scales will aid global efforts to restore tree cover to millions of hectares of degraded land. While optical satellite remote sensing can detect regional land cover change, quantifying forest structural change is challenging. We developed a state-space modeling framework that applies Landsat satellite data to estimate variability in rates of natural regeneration between sites in a tropical landscape. Our models work by disentangling measurement error in Landsat-derived spectral reflectance from process error related to successional variability. We applied our modeling framework to rank rates of forest succession between 10 naturally regenerating sites in Southwestern Panama from about 2001 to 2015 and tested how different models for measurement error impacted forecast accuracy, ecological inference, and rankings of successional rates between sites. We achieved the greatest increase in forecasting accuracy by adding intra-annual phenological variation to a model based on Landsat-derived normalized difference vegetation index (NDVI). The best-performing model accounted for inter- and intra-annual noise in spectral reflectance and translated NDVI to canopy height via Landsat–lidar fusion. Modeling forest succession as a function of canopy height rather than NDVI also resulted in more realistic estimates of forest state during early succession, including greater confidence in rank order of successional rates between sites. These results establish the viability of state-space models to quantify ecological dynamics from time series of space-borne imagery. State-space models also provide a statistical approach well-suited to fusing high-resolution data, such as airborne lidar, with lower-resolution data that provides better temporal and spatial coverage, such as the Landsat satellite record. Monitoring forest succession using satellite imagery could play a key role in achieving global restoration targets, including identifying sites that will regain tree cover with minimal intervention.

Key words: forest landscape restoration; hierarchical Bayes; Landsat time series; Landsat–lidar fusion; large-scale restoration; Latin America; natural regeneration; reforestation; spatial prioritization; state-space model; tropical forest succession.

Introduction

Across the tropics, secondary forests are regrowing on land that was previously cleared for agriculture (Rudel 2012, Chazdon 2014). These second-growth forests represent an enormous carbon sink, with potential to act as a natural climate solution while providing a suite of other ecosystem services (Griscom et al. 2017, Busch et al. 2019). Determining how to incorporate natural regeneration into national and international plans to restore forest cover to millions of hectares of degraded land is a top research priority (Chazdon and Uriarte 2016). However, outcomes of natural regeneration are highly variable between sites (Holl and Aide 2011, Norden et al. 2015, Shoo et al. 2016). For example, aboveground biomass in 20-yr old secondary forests can vary by over an order of magnitude (Poorter et al. 2016). This high variability in biomass recovery is a significant challenge for incorporating natural regeneration into forest restoration plans and points to an urgent need to understand rates of secondary succession across heterogeneous landscapes.

Logistical considerations limit the spatial extent of field studies of natural regeneration, potentially leading

Manuscript received 26 February 2020; accepted 4 May 2020. Corresponding Editor: Yude Pan.
[8] E-mail: trevorcaughlin@boisestate.edu

to biased estimates of landscape-scale forest dynamics from forest inventory plot data (Marvin et al. 2014). Funding also constrains the timespan of field measurements, and lack of sufficient monitoring is a frequent problem for reforestation projects (Mansourian and Vallauri 2014, Evans et al. 2018). Field data gaps due to limited spatial and temporal coverage provide one explanation for high variability in the contribution of forest regrowth to global carbon sink dynamics (Pugh et al. 2019). The limited scale of field data raises the question of how well satellite remote sensing can measure forest succession over large areas and long time periods (White et al. 2019).

The primary source of remotely sensed data for measuring historical changes in land cover is the Landsat satellite archive, providing open access to >40 yr of globally extensive data (Zhu et al. 2019). Most studies have applied Landsat imagery to quantify forest recovery either as a transition between discrete land cover categories or as trajectories of spectral recovery, typically vegetation indices. Linking either of these methods to an ecological interpretation of forest structural change is problematic. Land cover change studies that define reforestation as a transition from non-forest to forest pixels (Aide et al. 2013, Sloan 2015, Schwartz et al. 2017), oversimplify the ecological dynamics of secondary succession, an inherently continuous process (Song et al. 2002, Caughlin et al. 2016*b*, Coops and Wulder 2019). In contrast, vegetation indices (VI), such as the Normalized Difference Vegetation Index (NDVI), present a continuous proxy for ecosystem structure and function (Pettorelli et al. 2005, Requena-Mullor et al. 2018). VIs are straightforward to calculate from satellite reflectance data and have been widely applied to track recovery in disturbed ecosystems (Kennedy et al. 2012, Dutrieux et al. 2016, Frazier et al. 2018). Nevertheless, VIs do not have a direct physical interpretation, and the relationship of these indices to forest structure during regrowth is not straightforward (Frolking et al. 2009).

The challenges of interpreting Landsat spectral reflectance in an ecologically meaningful way have prompted the development of statistical models that relate spectral reflectance to forest structure (Pflugmacher et al. 2014, Ota et al. 2014, Ahmed et al. 2015, Bolton et al. 2018). Most commonly, these statistical models are developed using lidar-derived metrics of forest structure as training data (Marvin et al. 2014, Lee et al. 2018, Ver Planck et al. 2018). Forest structural metrics estimated with high accuracy using lidar data include tree cover, height, and biomass (Almeida et al. 2019*b*). A recent study has demonstrated the potential for Landsat–lidar fusion to estimate forest structural dynamics at a national extent over multiple decades (Matasci et al. 2018). Recent work has also quantified how rates of spectral recovery relate to measures of forest structure derived from airborne lidar in boreal forests subject to disturbance (White et al. 2017). Because satellite-borne passive sensors such as Landsat predate the development of lidar technology, applying lidar-trained models to construct historical time series of forest structure from satellite data requires extrapolation (i.e., prediction outside the scope of the model). However, extrapolating Landsat–lidar fusion to years with no lidar data could lead to systematic error due to high variability in Landsat spectral reflectance from year to year.

The central problem is that temporal variation in medium-resolution satellite data has many causes that are unrelated to changes in forest structure, including illumination, signal-to-noise-ratio, phenology, and atmospheric conditions (Kennedy et al. 2010, Misra et al. 2018). While the development of atmospheric correction algorithms for surface reflectance has improved our capacity to extend Landsat-derived models through space and time (Song et al. 2001), inter- and intra-annual noise remains a major impediment to quantifying forest recovery with Landsat data (Verbesselt et al. 2010, Kennedy et al. 2012). In addition to high variability in spectral reflectance, missing data are also prevalent throughout the Landsat archive due in part to data storage problems and the scan line corrector (SLC) failure onboard Landsat 7 (Wulder et al. 2008). Pixel compositing approaches present one solution to missing data (Hermosilla et al. 2015), however, pixel-to-pixel variability can occur if composited images represent a combination of different vegetation phenologies. While missing data and noise complicate assessments of forest recovery using Landsat data, spectral reflectance is an imperfect proxy of forest structure, even in the best-case scenario. Across a range of study systems and statistical approaches, models based on Landsat spectral reflectance can explain ~60–80% of the variation in lidar-derived forest structure (Avitabile et al. 2012, Ota et al. 2014, Ahmed et al. 2015, Caughlin et al. 2016*b*, Matasci et al. 2018). These studies suggest inherent upper limits in the accuracy of forest structure measurements using space-borne passive sensors. Overall, distinguishing the signal of forest recovery from the noise of satellite spectral reflectance data is a daunting problem.

Fortunately, ecological science has a lengthy track record of inference from imperfectly observed data. State-space models provide a formal way to estimate the parameters of dynamic, process-based models while simultaneously accounting for measurement and process error (Clark and Bjørnstad 2004). For example, the Breeding Bird Survey is a continental-scale, multi-decadal data set of bird counts collected by citizen scientists. Similar to the Landsat satellite record, the Breeding Bird Survey presents opportunities for ecological inference over large scales and challenges due to multiple sources of uncertainty. By explicitly modeling abundance conditional on detection, state-space models have enabled researchers to use this extensive but noisy data set to explain the spread of invasive species (Hooten et al. 2007), map bird species richness (Dorazio et al. 2006), and forecast population trends (Schmidt et al. 2013). Other applications of state-space models for ecological

inference include estimating disease outbreaks with imperfect reporting rates (Cauchemez and Ferguson 2008), wildlife density from camera trap data (Royle et al. 2009), and demographic rates of tree seedlings censused in dense, weedy environments (Caughlin et al. 2019). However, state-space modeling has not been widely applied to satellite-borne remotely sensed data (Bernardis et al. 2015, Kellner and Hubbell 2017). We propose that state-space models complement previous studies of trends in land cover change (Coops et al. 2010, Kennedy et al. 2012, Hermosilla et al. 2015) by explicitly modeling both process and measurement error.

We applied state-space models to capture forest dynamics during early succession, using time series of Landsat spectral reflectance and a single snapshot of lidar data. Our primary objective was to rank successional rates across sites undergoing natural regeneration, corresponding to the practical challenge of prioritizing sites for active restoration. Our study takes place in a tropical region undergoing net increases in forest cover (Caughlin et al. 2016*b*). Within this region, we selected naturally regenerating sites and evaluated the performance of state-space models of forest succession fit to time series of Landsat-derived NDVI. We began with a state-space model built on a logistic growth process for forest structural change. We then developed increasingly complex models for measurement error, including accounting for intra-annual variation in the date of image acquisition and inter-annual variation in NDVI baselines. Building off the model that represents inter- and intra-annual variation in measurement error, we incorporate Landsat–lidar fusion to model canopy height dynamics. Within this set of models that vary in complexity and data requirements, we compare (1) model forecasting accuracy, (2) ecological inference on successional dynamics, and (3) ranking of successional rates between sites. Altogether, our modeling approach demonstrates a solution to the problem of quantifying variability in forest succession at landscape scales.

Methods

Regional context

Our study is located in Los Santos Province in Southwestern Panama (Fig. 1). Before European settlement, the region was characterized by tropical dry forest, with annual precipitation of 1,700 mm, an average temperature of 25°C, and a pronounced dry season from January to May. Regional-scale deforestation rates reached an apex during the early 20th century when ranchers cleared large areas of land for cattle production (Heckadon-Moreno 2009). During the past three decades, land cover change has shifted toward net reforestation, likely related to rural economic development and forest scarcity (Wright and Samaniego 2008, Sloan 2015). Currently, tree cover in the landscape is composed of a few small forest fragments and a variety of agricultural tree cover types, including dispersed pasture trees, live fences, and riparian corridors (Tarbox et al. 2018). A sizeable fraction of aboveground biomass is stored in trees outside forests (Graves et al. 2018). Previous field work in our study region has demonstrated that fifteen-years is a sufficient period of time to detect differences in metrics of succession between sites, including biomass accumulation and tree species richness (Estrada-Villegas et al. 2020).

Site selection

We selected sites for our analyses using a tree cover change data set derived from airborne photographs acquired in 1998 by the Tommy Guardia National Geographic Institute of the Republic of Panama and Google Earth images acquired in 2014. These very high resolution (≤0.5 m) data sets enable visualization of small patches of tree cover. Subsamples of these images were digitized to quantify tree cover change (Tarbox et al. 2018). The subsamples consisted of 150 × 150 m plots, each randomly located within a single property boundary (hereafter "Sites"). Sites were designed to overlap with Landsat 7 data, such that each site contained 25 Landsat pixels (Fig. 2). We selected 252 of these sites matched to the same ecoregion as an airborne lidar image (see below). For these 252 sites, we quantified the percent change of tree cover from 1998 to 2014 using the digitized polygons (available from Tarbox et al. 2019). Reference sites represent the entire range of cover types, from bare ground to active pasture to closed canopy forest. As the focus of this study was fitting models for forest succession, we selected the 10 sites with the highest increases in tree cover to use as focal sites for our subsequent analyses. The boundaries of the 252 reference sites and the 10 reforestation sites were used to clip Landsat data for our analyses; otherwise, we did not use the high-resolution data for model construction. For a summary of relationships between all data used in our modeling, see Fig. 3.

Landsat data

We extracted Landsat 7 data between 1 December and 31 March from 1999 to 2015. Similar to many other tropical forest sites, cloud cover during the rainy season restricts availability of imagery at our study area to the dry season. The period between December and March corresponds to the driest part of the year, resulting in less cloud contamination. Previous work at our study site has shown that compositing Landsat images from this time period results in better predictions of forest structure than any single scene alone (Caughlin et al. 2016*b*). We used surface reflectance data from the USGS Climate Data Record (*available online* via the USGS Earth Explorer interface),[9] processed using the Landsat

[9] https://doi.org/10.5066/F7WH2P8G

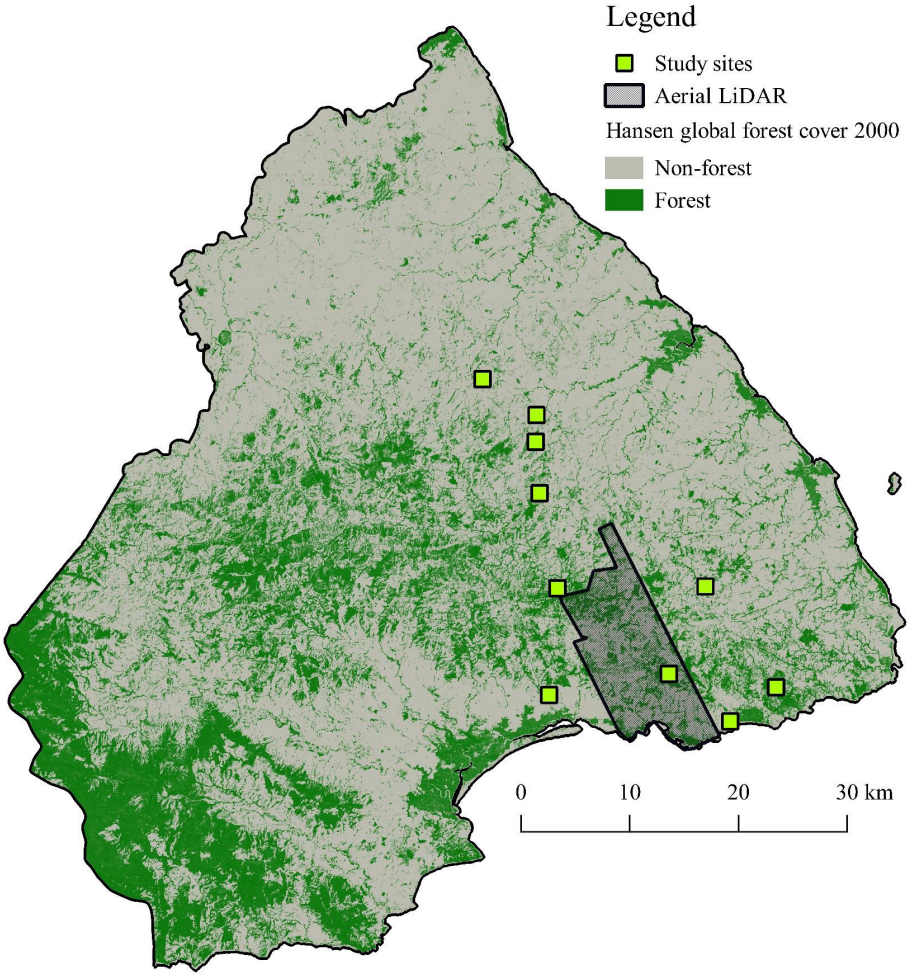

FIG. 1. Map of study area. Los Santos Province in Southwestern Panama.

Ecosystem Disturbance Adaptive Processing System (LEDAPS) algorithm (Masek et al. 2006). Cloud contaminated pixels were removed using the cloud mask band from the LEDAPS product (for more details, see Caughlin et al. 2016*b*). In total, this resulted in 58 Landsat scenes with a range of two scenes per year (2001 and 2011) to six scenes per year (2010), all from Path/Row 012/055.

Numerous vegetation indices have been proposed to monitor forest regrowth from Landsat spectral reflectance. NDVI has a long history of use and is the most familiar spectral index to a broad range of ecologists (Pettorelli et al. 2005). However, NDVI can be problematic as it saturates early during forest succession (Song et al. 2002). Alternative Landsat indices used to quantify forest regrowth include the Normalized Difference Water Index (NDWI; e.g., Chen et al. 2016) and the Normalized Difference Moisture Index (NDMI; e.g., Dutrieux et al. 2016). The Normalized Burn Ratio (NBR) incorporates Landsat's short-wave infrared band, which is highly sensitive to canopy moisture content, and has emerged as a powerful tool for quantifying forest succession (White et al. 2017, Nguyen et al. 2018). To determine which index was most appropriate for our study goals, we assessed the ability of several Landsat-derived indices, including NDVI, NDWI, NDMI, NBR, to predict lidar-derived canopy height in our study region (described in Appendix S1). Out of this set of normalized difference indices, we found that NDVI had the highest out-of-sample predictive accuracy (Appendix S1: Table S1). Relative to NBR, the next best-performing spectral index, NDVI increased R^2 by 4% and decreased RMSE by 0.15 m. In addition, all normalized difference indices tested exhibited spectral saturation at high values of canopy height (Appendix S1: Fig. S1). Therefore, we selected NDVI as the primary response variable for this study. Nevertheless, we emphasize that the best-fit vegetation index for canopy height data may vary between study regions and should be selected with care.

We produced annual composites of Landsat images by taking the average NDVI per pixel stack per year. The particular dates used to construct annual composites

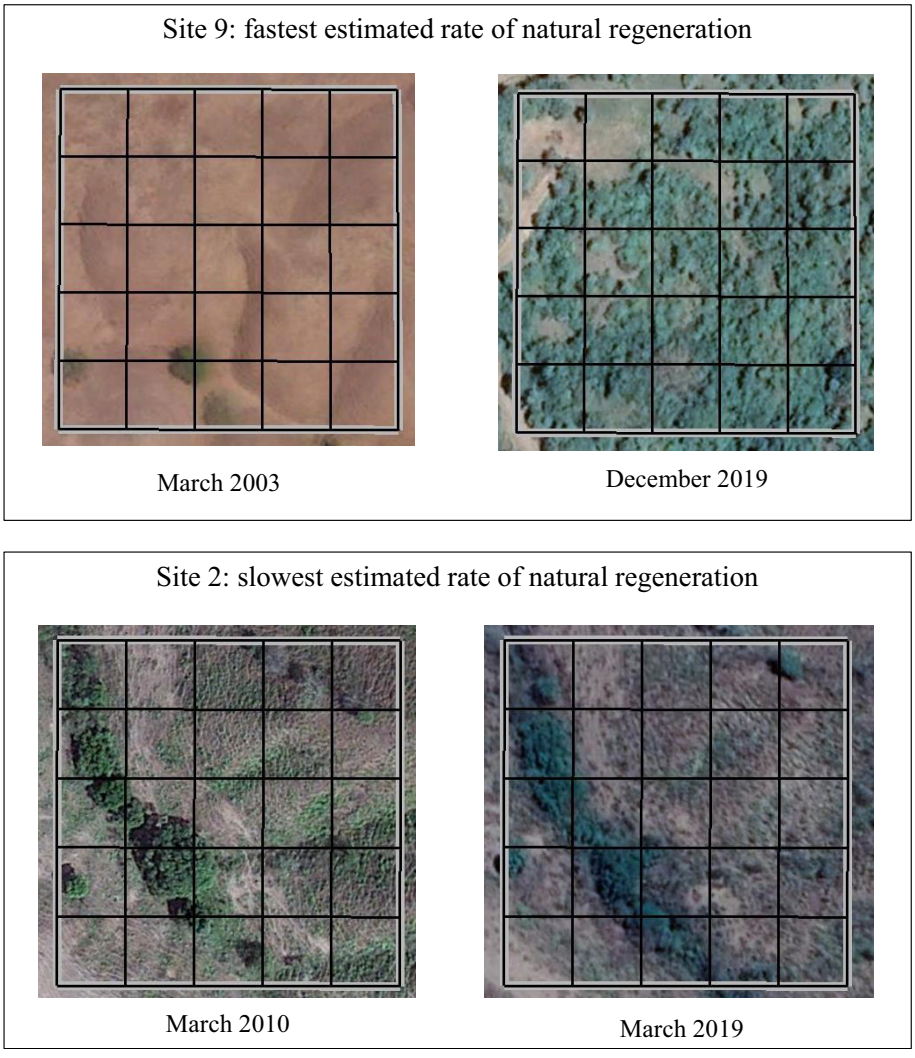

FIG. 2. Regeneration in two 150 × 150 m sampling units between 2003 and 2019. Gridlines represent 30-m Landsat pixels. Rates of natural regeneration and site numbers correspond to Table 1. Images courtesy of Google Earth.

varied at the pixel-level, due to pixel-level variation in missing data. We excluded pixels with more than one consecutive missing value between years (<6% of the full data set). The end product of Landsat processing was a fifteen-year time series of NDVI across our study region.

Lidar data

The Carnegie Airborne Observatory-2 (now the Global Airborne Observatory) collected lidar data on 11 January 2012, using a dual-laser waveform scanner with a density of 2 points/m^2. We developed a canopy height model (CHM) with the classified point-cloud data with a pixel size of 1.13 m covering a 13,333-ha area (Asner et al. 2013). CHM pixels were resampled to match the extent of Landsat pixels using bilinear interpolation, resulting in a total of 676 CHM pixels of ~1.15 m^2 within each 30-m Landsat pixel.

Process model

The goal of our modeling efforts was to fit a logistic growth model for forest regrowth using the Landsat time series while accounting for variance in spectral reflectance unrelated to forest structural change. We implemented the logistic growth model as our ecological process model for several reasons. This model has a long history for modeling population dynamics (Tsoularis and Wallace 2002, Zelnik et al. 2019). Similar models have been widely applied to represent the latent dynamics of population growth in state-space models (Clark and Bjørnstad 2004, Dennis and Ponciano 2014, Nathan et al. 2015, Montenegro and Branco 2016). The logistic growth model has also been applied to forest dynamics, including diffusion models for spatial patterns of forest succession (Acevedo et al. 2012, Richit et al. 2019). The parameters in the logistic growth model are

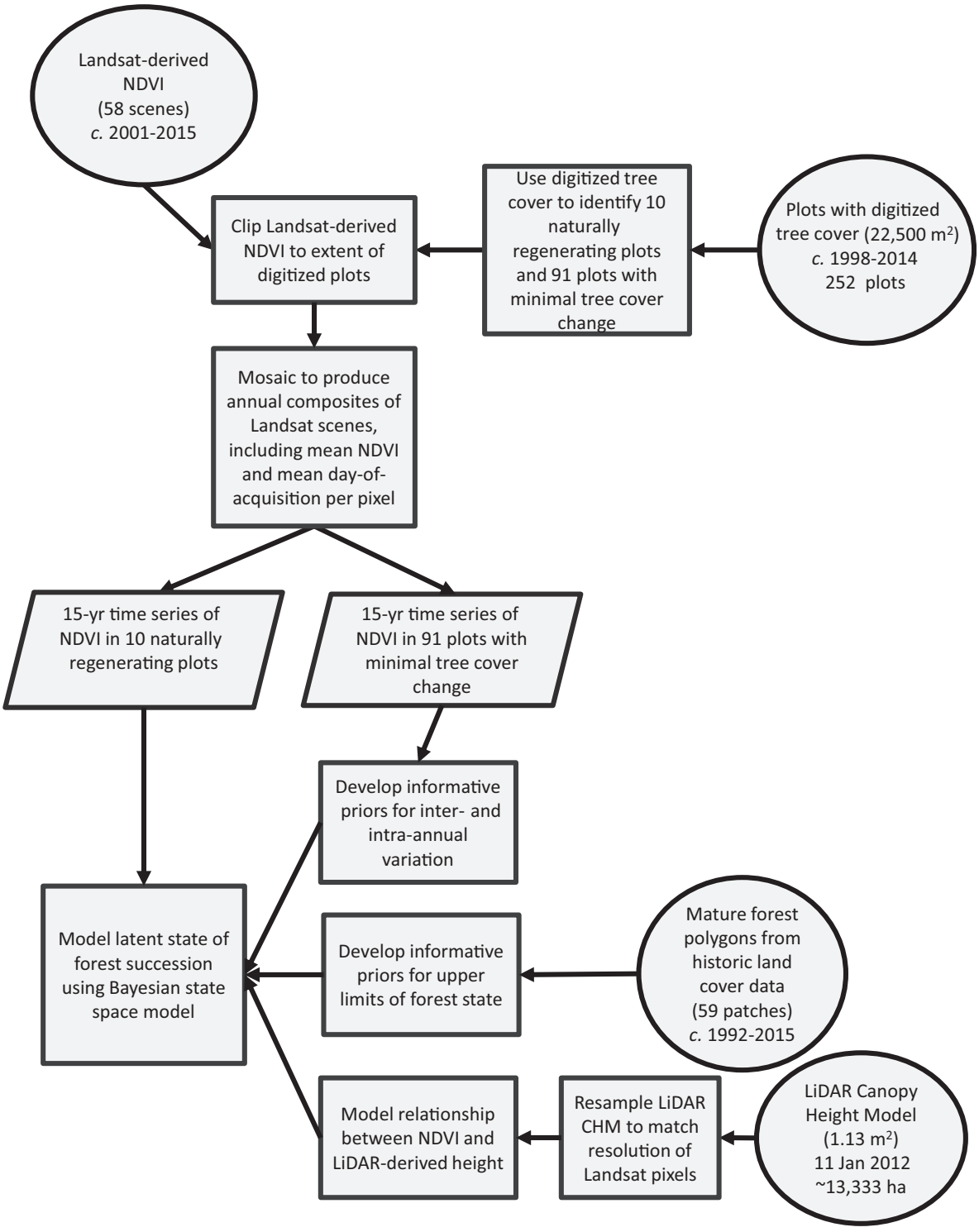

FIG. 3. Workflow for developing state-space model. Circles indicate input data, parallelograms indicate derived products, and squares indicate processes.

straightforward (Eq. 1) and include an intrinsic growth rate (r) and a "carrying capacity" (K). We consider K as the state of a mature secondary forest in our study region and did not allow K to vary between sites. In contrast, because our primary goal was to develop estimates of r to distinguish between sites undergoing different rates of forest succession, we enabled r to vary between our 10 reforesting sites

TABLE 1. Uncertainty in site ranking of successional rates between four state-space models.

Model	Measurement error	Most frequent site ranking	Draws (%)	*P* (S9) best	*P*(S2) worst
Basic	no covariates	S2 < S4 < S6 < S8 < S7 < S1 < S5 < S3 < S9 < S10	1.1	0.42	0.46
Intra-annual phenology	date of acquisition	S2 < S6 < S7 < S1 < S4 < S3 < S8 < S5 < S10 < S9	1.7	0.89	0.77
Inter- and intra-annual phenology	date of acquisition + year	S2 < S6 < S7 < S1 < S4 < S3 < S8 < S5 < S10 < S9	1.4	0.90	0.79
Canopy height	date of acquisition + year + Landsat-lidar fusion	S2 < S6 < S7 < S1 < S4 < S3 < S8 < S5 < S10 < S9	5.6	0.89	0.74

Notes: The most frequent site ranking column represents the ranking (from slow to fast) of successional rate between the 10 sites in our study, with the letter S preceding the number of the site. Fig. 2 illustrates the sites numbered S2 and S10. The percentage of draws column represents the percentage of draws from the HMC algorithm with the same ranking of sites. The *P*(S9) best and *P* (S2) worst columns represent the probability that site 9 and site 2 were identified as the fastest and slowest regenerating sites. A higher probability of identifying a site as the best or worst site for natural regeneration indicates more certainty in model-produced rank orders.

$$S_{t+1} = S_t + rS_t\left[1 - \frac{S_t}{K}\right]. \quad (1)$$

The state variable S is subject to process error, as our logistic growth model is an imperfect representation of the ecological process of forest succession. We quantified process error using a normal distribution, with a variance parameter specific to state-space (σ_{ss}). In addition, we modeled the intrinsic growth rate r and the initial condition at the start of the study period (S_1) as site-level random effects, each drawn from a normal distribution. These site-level random effects account for non-independence between pixels from the same site. Altogether, our process model represents forest recovery in the ith pixel in the jth site at year y as

$$S_{i,j,y+1} \sim \text{Normal}\left(S_{i,j,y} + r_j S_{i,j,y}\left[1 - \frac{S_{i,j,y}}{K_j}\right], \sigma_{ss}\right). \quad (2)$$

Observation models

We developed four models with increasing complexity, beginning with a model that represents forest structure using NDVI with no covariates for measurement error (basic model), then progressively adding covariates, including date of acquisition (intra-annual phenology model), year-to-year effects (inter-annual phenology model), and finally, Landsat–lidar fusion to translate NDVI into canopy height (height model).

Basic model.—Our models for measurement error relate observations of NDVI at pixel i, site j, and year y, to latent variable S. For the first three models, we do not explicitly define S in terms of forest height. Instead, we consider state variable S to represent a "true" NDVI, without the complications of different date of acquisition between years (variation due to phenology), sensor failure, unremoved atmospheric differences, and other sources of measurement error. To represent those sources of noise, we model observed NDVI as draws from a normal distribution with S as the mean value and a variance term, σ_{obs}. The magnitude of σ_{obs} directly represents measurement error. Due to identifiability problems, we were not able to estimate the variance term for the process model (σ_{ss}) as a free parameter in our basic model; instead, for the basic model only, we set this parameter equal to 0.01, based on initial simulations of the process model. Results were robust to different values of this parameter. For all other models, we estimated σ_{ss} from the data

$$\text{Basic model:} \quad \text{NDVI}_{i,j,y} \sim \text{Normal}(S_{i,j,y}, \sigma_{obs}). \quad (3)$$

Intra-annual phenology.—Our Landsat data encompass the onset of the dry season in December to the end of the dry season in late March. During this period, deciduous trees lose their leaves, and herbaceous vegetation dries up, leading to a "brown-down" signal that is evident in satellite imagery (Bohlman 2010). Limiting our Landsat images to this period simplifies intra-annual phenology, as the browning-down process is approximately linear during this period (Appendix S2: Fig. S1). For each pixel from the annual NDVI composite, we calculated average date of acquisition. This date of acquisition predictor variable varies within and between years, due to varying annual dates of Landsat image acquisition and to different dates with missing data in annual pixel stacks. For example, if one year was represented by a total of three Landsat scenes, the average NDVI for that year for a particular pixel could represent the average of any combination of those three scenes. The average date of acquisition varies at a pixel scale because scene-specific patterns of missing Landsat data are spatially variable. To enable better integration of the state-space model with the lidar data, we centered date of acquisition around the day of lidar acquisition (11th

January), such that the date of acquisition was equal to zero for this date. As a result, positive and negative values of date of acquisition represent the number of days that the average date of acquisition per pixel differed from 11th January. We then fit an observation-level model that included date of acquisition as a linear predictor variable ("Day" in Eq. 4). This observation model accounts for pixel-level variability in greenness due to within-year phenology that is separate from forest structural change (represented by $S_{i,j,y}$ below).

$$\text{Intra} - \text{annual model}: \quad \text{NDVI}_{i,j,y} \sim \text{Normal}(S_{i,j,y} + \beta\text{Day}_{i,y}, \sigma_{\text{obs}}). \tag{4}$$

Inter-annual phenology.—In addition to within-year phenological change, we expected that different years would have different "baseline" levels of greenness (Reed et al. 1994). We accounted for inter-annual variability using a categorical variable to represent years, with a separate estimate of this fixed effect for each year (γ_y). We set $\gamma_{2012} = 0$, such that the year of lidar acquisition (2012) functions as our baseline year to which all other years are compared. We consider the year effect as interannual variation in greenness unrelated to successional change, and constrained estimation of γ_y using informative parameters derived from sites that exhibited minimal change in tree cover during the study period (see *Priors* subsection for more details).

$$Inter - annualmodel: NDVIi, j, t \sim Normal (Si, j, t + \beta Dayi, t + \gamma t Yeart, \sigma obs). \tag{5}$$

Landsat–lidar fusion.—For our final model, we converted NDVI into lidar-derived canopy height. We first developed a statistical model to relate the Canopy Height Model to Landsat data from 2012 (Eq. 6). This model structure is a generalized linear model (GLM) with gamma distributed errors and a log-link function, following Caughlin et al. (2016*b*). In addition to NDVI as a predictor of canopy height, we included average date of acquisition per pixel for the 2012 data. This term accounts for variations in greenness within a year due to date of image acquisition, a source of variability that we assume is unrelated to tree height. As input to the lidar-Landsat model, we randomly sampled 4,000 pixels from the matched Landsat and the resampled Canopy Height Model. We jointly estimated the slope and intercept parameters (*a* and *b* in Eq. 6) as components of the state-space model (Eq. 7), where the *k* subscript represents the *k*th pixel out of the set of 4,000 used to train the Landsat–lidar model.

$$\text{HT}_{2012,k} \sim \text{Gamma}\left(\theta, \frac{\theta}{\exp[a + b\text{NDVI}_{2012,k} + d\text{Day}_{2012,k}]}\right). \tag{6}$$

An advantage of jointly estimating parameters *a* and *b* in Eqs. 6 and 7 is that uncertainty in these parameter values is propagated to predictions for canopy height across the 15-yr time series. A potential disadvantage of joint estimation is that information from the time series could "feed back" into the estimation of the Landsat–lidar parameters, leading to unreliable parameter estimates (Plummer 2015). To test how joint estimation impacted predictions from the Landsat–lidar model, we compared out-of-sample accuracy between the jointly estimated GLM and the same GLM fit independently of the state-space model (i.e., using only data from 2012). Our out-of-sample test data consisted of all resampled pixels from the Canopy Height Model not used to fit the GLM (n = 26,162).

The final step in our joint modeling approach was to predict observed NDVI from the time series of latent canopy height. Eq. 7 shows how we applied the intercept and NDVI-slope parameters (*a* and *b*) to translate the latent state variable $S_{i,j,t}$, representing canopy height, into observed NDVI at a particular date of acquisition and year

$$\text{Height model}: \quad \text{NDVI}_{i,j,y} \sim \text{Normal}\left(\frac{[\log(S_{i,j,y}) - a]}{b} + \beta\text{Day}_{i,y} + \gamma_y\text{Year}_y, \sigma_{\text{obs}}\right).$$

Parameter estimation

Priors.—Fitting our models in a Bayesian framework enabled us to take advantage of prior data for several parameters in our model. For our observation models, representing variation in spectral reflectance unrelated to forest structural change, we incorporated data from reference sites in areas with minimal tree cover change during our study period. These reference sites were determined using sites from the same study used to identify reforesting sites (Tarbox et al. 2018) with less than 3% absolute change in tree cover from 1998 to 2014, quantified through a detailed examination of airborne imagery. There were a total of 91 sites that met this criterion. For each of these reference sites, we extracted NDVI values from Landsat 7 surface reflectance data and fit a model that included inter- and intra-annual variation. For these models, we used pixel-level NDVI as a response variable with the date of acquisition and year variables as continuous and categorical predictor variables. We also included site identity as a random effect to account for possible spatial autocorrelation in spectral reflectance from pixels within the same site. We fit these linear mixed-effect models corresponding to observation models in Eqs. 4, 5 using the rstanarm package with default priors (Goodrich et al. 2020). We then used the mean and standard deviation of parameter estimates from the linear mixed effect models to construct informative priors for the β, γ_y, and σ_{obs} parameters in our state-space models. Overall, this approach enabled us to leverage prior information on Landsat spectral variability in the verified absence of forest structural change.

The other parameter we were able to constrain using prior data was the *K* parameter in our process model for

forest dynamics. In the logistic growth model, this parameter represents carrying capacity; in the context of forest succession, we consider this parameter as the NDVI saturation or maximum canopy height of mature secondary forest in the region. To develop priors for K, we identified patches of mature secondary forest in our study landscape. We started by extracting secondary forest polygons from a data set representing land cover in 1992, developed at the Landsat scale by Panama's Ministry of the Environment. We then overlaid these secondary forest units on Google Earth images taken in 2015, and manually digitized areas that were classified as secondary forest in 1992 and still were dominated by forest in 2015. This overlay resulted in 59 different patches of mature secondary forest, with a total of 1,169 30 × 30 m Landsat pixels across all mature secondary forest patches. We calculated beta-distributed informative priors for K in the basic, intra- and inter-annual models using Landsat-derived NDVI from 2001 to 2015. We then used beta regression (Zeileis et al. 2018) to calculate the expected value for NDVI in an intercept-only model (corresponding to the basic observation model), a model with average date of acquisition as a sole predictor variable (corresponding to the intrannual model), and a model with both day and year as predictor variables (corresponding to the inter-annual model). For the height model, we calculated gamma-distributed informative priors for K using the CHM aggregated to the 30 × 30 m Landsat scale, with pixels clipped to the digitized mature secondary forest polygons. Because the CHM represents forest structure at a single date (11 January 2012), we did not include covariates for date of year or year in this model. Altogether, our efforts led to four sets of informative priors, corresponding to our four models. We report prior distributions for parameters in Appendix S3.

Estimation.—Model fitting was conducted via Hamiltonian Monte Carlo (HMC) algorithm in the Stan programming language (Stan Development Team 2016). Stan model code for our four models is available online (see *Data Availability*; Caughlin and Wilson 2020). For each of our four models, we ran 12 chains for 6,000 iterations, discarding the first 4,000 iterations of each chain as warm-up, leaving 24,000 samples for estimating posterior distributions. We assessed convergence by visual examination of the chains, and through checking of the unique diagnostics from HMC (Betancourt 2017). We summarize posterior parameter estimates in Appendix S3.

Model evaluation.—We evaluated model performance by quantifying uncertainty in site rankings between models and by testing the ability of models to forecast NDVI trajectories. A primary goal of our modeling approach is to confidently discriminate between sites that are recovering forest structure quickly and those that are recovering more slowly. To determine how different models achieve this goal, we compared site rankings of the r parameter (Eq. 1) between models. We took advantage of posterior draws from our Bayesian models to propagate uncertainty from model estimation to site rankings. For each iteration of our HMC output, we created a vector representing the order of the r parameter for each site. In other words, each HMC iteration contains a single draw of the r parameter for each site, which can be arranged into an ordered vector $\{r_1, r_2, \ldots r_{10}\}$. Because our output included 24,000 posterior draws, we had a total of 24,000 ranked orders for each fitted model. We then evaluated the frequency distribution of the various site rankings, by summing the number of times that a specific sequence $\{r_i\}^{10}$ appears over 24,000 draws. We interpreted the relative frequency of the most common rank order as a measure of certainty in site rankings.

The relative frequency of rank orders between models of successional rate provides information on model precision but rank orders alone do not indicate whether Landsat-derived estimates accurately measure successional change. To validate our modeled successional rate estimates, we compared our results to percentage change of tree cover derived from digitized high resolution imagery (Tarbox et al. 2019). While these digitized tree cover data were used to identify sites that were undergoing succession, data on relative rates of succession from these sites were not used in model construction and can be considered independent data. To validate the relative successional rates from our models, we extracted the r parameter (Eq. 1) for each site from model predictions, including 24,000 posterior draws for each site's value of r from each model. We then matched each r parameter to the percentage change of tree cover from each site. We did not expect a one-to-one relationship between the Landsat-derived r parameter, which reflects change from about 2000 to 2015, is unconstrained, and represents NDVI or canopy height, and the high resolution imagery-derived percentage of tree cover change, which reflects change from 1998 to 2014, is constrained between −1 (100% tree cover loss) and 1 (100% tree cover gain), and represents tree canopy cover. Consequently, we applied Pearson's correlation coefficient to ask whether there was a correlation between the two metrics of successional change, rather than directly evaluating error between observed and predicted values. We considered positive correlations between the r parameter and percentage tree cover change as an indicator that our model-based inferences successfully reflect relative rates of forest succession.

As a separate model validation exercise, we tested model forecasting ability by quantifying how well models fit with data from the first 12 yr of the time series could predict observed NDVI three years later. For data with spatial and temporal structure, thoughtful consideration of what data are held out is key to ensuring that model evaluation matches objectives for model use

(Roberts et al. 2017). We chose to hold out the last three years of data for all sites for model validation as a test of how well our logistic growth model can forecast NDVI trajectories. Predicting the final three years of the data out-of-sample corresponds to the applied need to predict vegetation dynamics into the future. We calculated forecast error as root mean square error (RMSE), relative RMSE, and bias between observed NDVI and forecasts of NDVI in 2015. Because the slope for the date of acquisition predictor variable representing phenology (β in Eq. 4) is constant across years, we incorporated date of acquisition as a variable in model forecasts. In contrast, our modeled effect of year-to-year variation (γ_y in Eq. 5) is unknowable in advance, and we did not incorporate year as a variable in model forecasts. Thus, our forecasts assume that future years have the same effect on measurement error as our baseline year of 2012 when lidar data was acquired.

Results

Dynamics of NDVI

In our 10 reforesting sites, the Landsat-derived NDVI time series data exhibited net increases in vegetation cover during the study period, including higher values of NDVI in 2015 than in 2001 for nearly all pixels (97.74%). Along with the trend of increasing NDVI over time, the Landsat data exhibited considerable inter-annual variation (Fig. 4). Six out of 15 years had an average decrease in NDVI, with the largest decline in 2004. The variance between years (mean coefficient of variation: 0.203) was higher than the variance between pixels in the same year (mean coefficient of variation: 0.158), demonstrating how temporal variation in observed NDVI overwhelmed spatial differences across our 10 sites.

Observation models

Our models suggest that intra-annual phenology explains a considerable portion of temporal variation between annual NDVI composites. Predictions from the basic model, with no temporal covariates in the observation model, failed to reproduce the peaks and valleys in the Landsat time series. The addition of a single linear covariate, average date of acquisition for each pixel in the annual NDVI composite (intra-annual phenology variable), resulted in predictions that qualitatively reproduced the observed data, including the timing and amplitude of stochastic year-to-year variation in NDVI trajectories (Fig. 4). This result suggests that much of the noise in the NDVI time series was due to varying dates of image acquisition during the progression of the dry season, rather than a signal representing vegetation structure. The date of acquisition covariate also likely improved model fit by correcting error due to the scan-line-corrector (slc) failure in Landsat 7 (Appendix S4; Fig. S1). While we found evidence for inter-annual variation in baseline NDVI, including different parameter estimates for each year, adding the year term did not

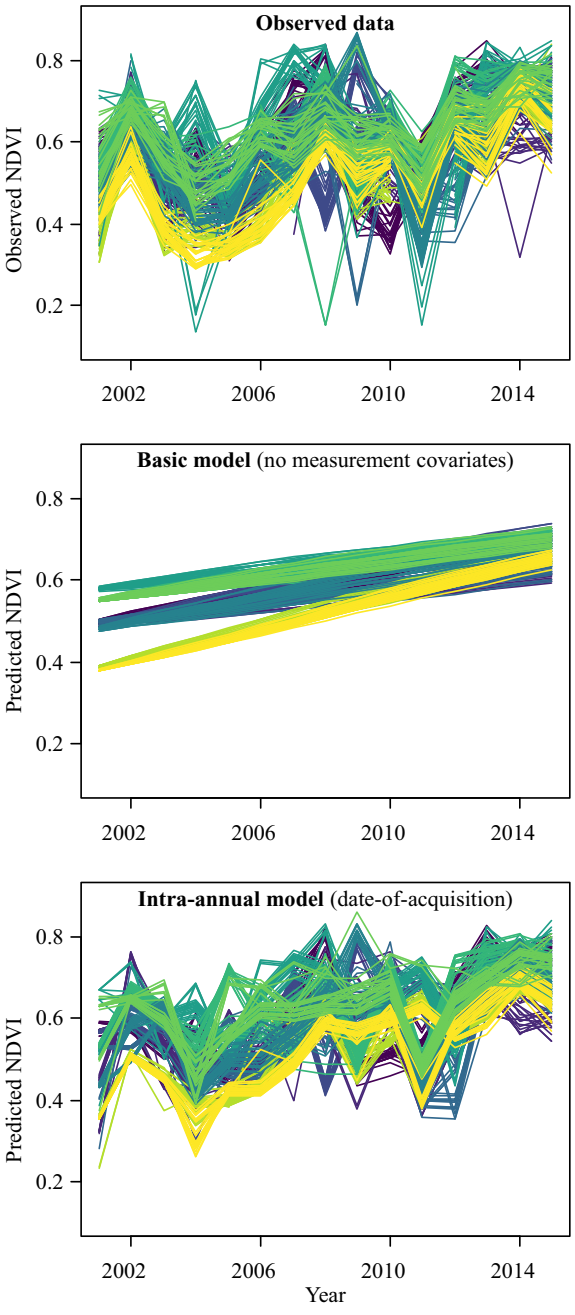

Fig. 4. Accounting for intra-annual variation in state-space models reproduces temporal patterns in observed data. These figures show observed and predicted NDVI over the ~15 yr from 2001 to 2015. Each line represents the trajectory of one pixel. Different colored lines represent different sites. The top panel shows observed NDVI from annual composites of Landsat 7 data. The middle and bottom panels show predicted NDVI from models. Results from all models are shown in Appendix S1: Fig. S3.

substantially alter predicted trajectories of NDVI (Appendix S5; Fig. S1).

Process models

Estimated rates of forest succession from the logistic growth model changed depending on which observation model was used. Between the three models for latent NDVI (basic, intra-annual, and inter-and intra-annual effects), successional rate (r) was highest for the basic model, with a median of 0.04 (95% CI 0.02–0.05) and lowest for the inter-annual model, with a median of 0.01 (95% CI 0.00–0.02). This result suggests that without accounting for inter-and intra-annual variability, models for successional change fit with Landsat data may lead to biased inferences, in this case, over-estimating successional recovery. In contrast to successional rate (r parameter in Eq. 1), maximum NDVI (K parameter in Eq. 1), was remarkably similar between models, with posterior median estimates between 0.91 and 0.92 (Appendix S3: Table S3).

We found fundamental differences in apparent successional dynamics between the model with latent height and the models with latent NDVI. The latent height model suggests accelerating rates of successional change for reforesting pixels, with minimal change early in the time series followed by major increases in height later in the time series. In contrast, the latent NDVI models suggest decelerating rates of change, with most change occurring early in the time series. We illustrate the differences in inferred successional dynamics between latent height and NDVI models through trajectories forecasted for 50 yr into the future (Fig. 5). The best fit model for latent NDVI begins with initial values relatively close to saturation. By 2030, NDVI values of pixels in this model exhibit decelerating growth rates as they approach the asymptote at $K = 0.92$. In contrast, the model for latent height begins with initial height values <5 m, far from maximum height at $K = 31.52$. By 2030, canopy height values have not yet reached the maximum growth rate at $K/2$, and many pixels still exhibit accelerating growth rates. Altogether, these results demonstrate that accounting for nonlinearity in the relationship between spectral indices and forest structure can substantively change inference on forest dynamics.

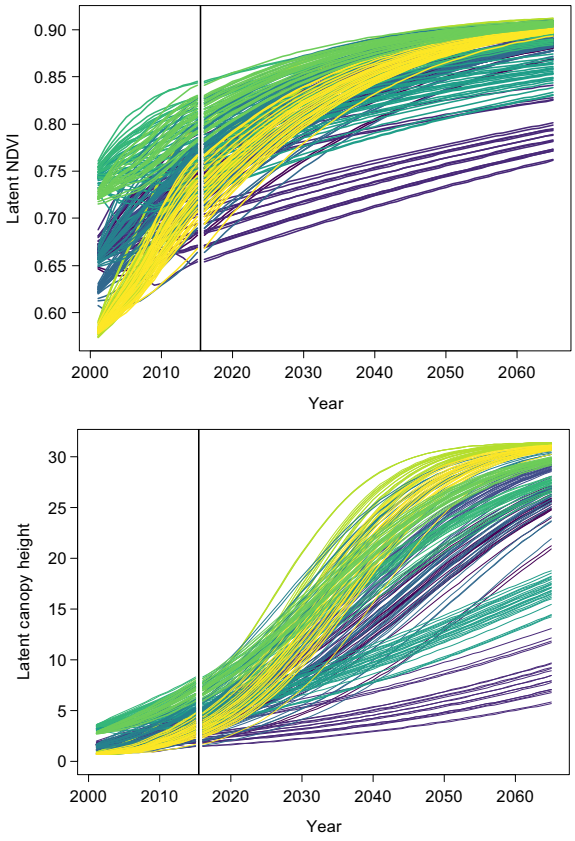

FIG. 5. Different ecological dynamics between state-space models with NDVI (top panel) vs. canopy height (bottom panel) as latent variables. The vertical line at 2012 divides the time series into observed and forecasted trajectories. Each colored line represents one pixel trajectory over the study period. Different colors represent different sites.

Variation in successional rate between sites

All models ranked site 2 as the site with the slowest rate of succession and site 9 or 10 as the site with the fastest rate of succession (Table 1; Fig. 2). There was a clear difference between the "basic" model with no covariates for measurement error and all other models in uncertainty surrounding sites with slowest and fastest natural regeneration: the addition of any covariates for measurement error nearly halved uncertainty in identifying best and worst performing sites. Models also identified different rank order of all sites. Namely, the latent height model outperformed all other models in the consistency of site rank order between HMC model iterations. While the most frequent rank order of sites was similar between the date of acquisition, year, and height models, the height model identified the most frequent rank order with nearly five times more certainty than the other models. For the top 50 site rank orders, the height model had a higher relative frequency of site rank orders compared to the NDVI-only models (Fig. 6). This result indicates greater certainty in identifying which sites are reforesting faster or slower when canopy height, rather than NDVI, was modeled as a response variable.

Validation of relative successional rates using percentage tree cover change from digitized imagery revealed that adding covariates for measurement error improved model performance (Fig. 7). The basic model with no covariates for measurement error had the weakest correlation with percentage tree cover change with a median value for Pearson's correlation coefficient of 0.08 and nearly one-fifth of the correlation coefficients were less than zero for this model, indicating little agreement

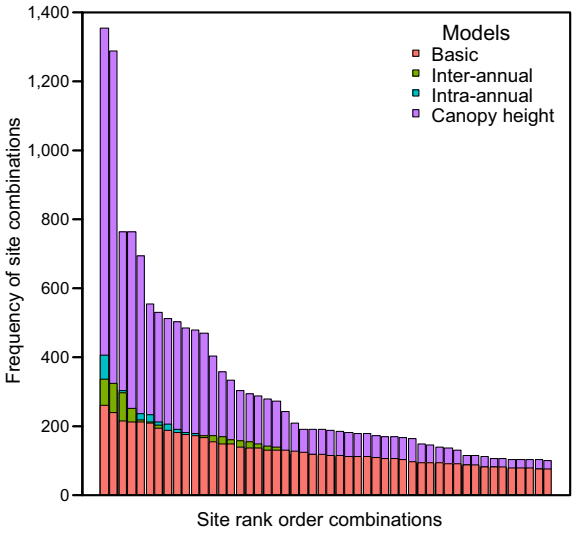

FIG. 6. Canopy height model increases certainty in rankings of natural regeneration rates across 10 sites. Each bar represents the number of times a rank order occurred in iterations of the Hamiltonian Monte Carlo (HMC) algorithm used to fit models to data. For clarity, we only show the top 50 rank combinations for each model.

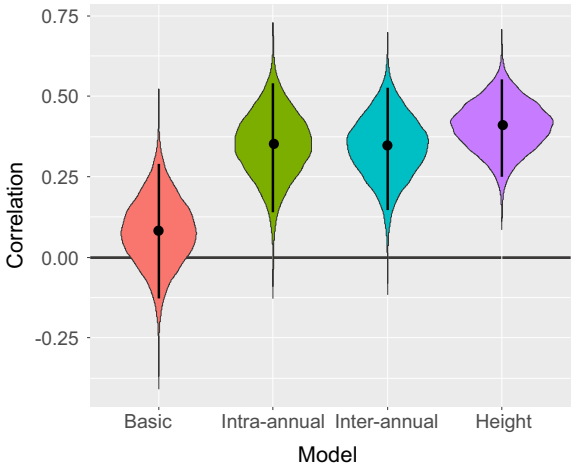

FIG. 7. Accounting for measurement error improves correlations between Landsat-derived successional rates and percentage tree cover change from digitized imagery. Violin plots indicate the posterior probability density of Pearson's correlation coefficient, calculated between posterior draws of Landsat-derived successional rate and percent tree cover change. Dots and lines inside posterior density represent the median and 95% CI of correlation coefficients. Correlations above zero (indicated by the black line) suggest agreement between the two metrics of forest succession.

between observed and modeled rates. In contrast, the median correlation between successional rate metrics was 0.35 for the date of acquisition model, 0.35 for the year model, and had the highest value for the height model, with a median correlation of 0.41. While all 24,000 posterior draws of successional rate from the date of acquisition, year, and height models had a positive correlation with percentage tree cover change, there was much less uncertainty in correlations for the height model. Altogether, the fit of different models for relative successional rate to percentage tree cover change exhibited similar patterns to the consistency of site rank order between models.

Comparison of forecast accuracy between models

Accounting for inter- and intra-annual variation as sources of measurement error improved the ability of models to predict NDVI over a 3-yr forecast horizon (Table 2). The biggest improvement in forecast accuracy occurred when intra-annual variation was added to the state-space model; the addition of a single parameter representing date of acquisition halved RMSE, relative to the model with no covariates in the measurement term. In comparison, adding terms to represent inter-annual variation only resulted in minor improvements to forecast accuracy. Without accounting for inter-annual variation, models tended to overpredict NDVI, while models that included inter-annual variation tended to under-predict NDVI.

The state-space model that represented latent canopy height, rather than latent NDVI, performed slightly better than the inter-annual model without Landsat–lidar fusion. The Landsat–lidar fusion model performed well despite uncertainty in the relationship between NDVI and lidar-derived canopy height, including a median RMSE of 4.20 m (95% CI 3.98–4.6 m) for the gamma GLM used to translate NDVI to canopy height. We did not find strong evidence that embedding the gamma GLM within the state-space model degraded the GLM's predictive accuracy, with similar RMSE for a gamma GLM fit independently of the Landsat time series (4.12 m; 95% CI 3.90–4.46 m).

DISCUSSION

Monitoring rates of forest succession at landscape scales will play a critical role in plans to reforest millions of hectares of degraded land. Earth-observing satellites present an opportunity to scale-up monitoring efforts, but detecting succession from medium-resolution satellite data is challenging, due in part to uncertainty in the relationship between satellite spectral reflectance and forest structural change. We demonstrate how hierarchical Bayesian models can improve our ability to quantify forest succession with satellite imagery by disentangling spectral noise and ecological process. We tested how accounting for measurement error in models for forest succession impacts ecological inference and forecasting ability. We found that modeling intra-and inter-annual noise in Landsat spectral reflectance substantially improved model forecasts. Translating spectral reflectance to canopy height via a Landsat–lidar fusion model resulted in better precision for ranking rates of natural

Table 2. Forecast error between observed NDVI and predicted NDVI for a 3-yr forecasting window (2013–2015).

Model	Measurement error	RMSE	Relative RMSE	Bias
Basic	no covariates	0.16 (0.14–0.17)	33% (28–38%)	0.09 (0.08–0.11)
Intra-annual phenology	date of acquisition	0.08 (0.07–0.09)	13% (11–14%)	0.01 (0.0–0.02)
Inter- and intra-annual phenology	date of acquisition + year	0.07 (0.07–0.08)	10% (10–11%)	−0.01 (−0.02 to 0.0)
Canopy height	date of acquisition + year + Landsat–lidar fusion	0.07 (0.06–0.08)	10% (8–11%)	−0.01 (−0.02 to 0.0)

Notes: Forecasting error was calculated as root-mean square error (RMSE), relative RMSE, and bias at the pixel-level. We propagated uncertainty in forecasts using posterior samples from the HMC algorithm, and present uncertainty as the median forecast error with 95% credible intervals in parentheses.

regeneration between sites, relative to NDVI-only models. Our approach has direct relevance for calls to jumpstart forest landscape restoration by identifying sites that can recover naturally with minimal human intervention (Chazdon and Uriarte 2016, Griscom et al. 2017). In our model framework, these correspond to sites with faster rates of canopy height growth, while sites showing minimal increases in canopy height may be more suitable for active restoration, such as tree planting.

At our study site in Southwest Panama, time series of annual NDVI composites exhibit high temporal variability unrelated to forest structural changes (Fig. 4). In contrast to field studies that repeatedly demonstrated high spatial variability in tropical forest succession at landscape scales (Norden et al. 2015, Poorter et al. 2016), temporal variability in NDVI measurements eclipsed spatial variation across our >380-km^2 study area. A major source of temporal variation in our data was intra-annual variation generated by different dates of image acquisition across years and missing data within years. We accounted for intra-annual variation using average date-of-image-acquisition as a covariate to explain measurement error. While other models for phenological change in satellite imagery span a range of complexity, including complex nonlinear functions (Zhu et al. 2012, Senf et al. 2017), we were able to approximate phenological change with a simple linear term. This linear approximation was possible by restricting image acquisition from the beginning to the middle of the dry season, corresponding to the period in which deciduous trees gradually lose their leaves in our study system. Altogether, modeling intra-annual variability provided the largest relative increase in model forecasting strength and improved our ability to discriminate between sites with slow vs. fast recovery rates. The generality of this approach will depend on whether similar periods of linear phenological change can be identified across other regions. Future work could evaluate other metrics to represent intra-annual variation, in addition to date of image acquisition, such as variance in spectral index and/or direct measurements of atmospheric conditions. The choice of multispectral vegetation index is also important for ecological inference on forest dynamics (Schroeder et al. 2011). In our study region, NDVI provided a better fit to canopy height data than other vegetation indices (Appendix S1). In other forest types, metrics that account for canopy moisture, such as the Normalized Burn Ratio (White et al. 2017), may be better metrics of forest recovery.

Inter-annual variation in average NDVI values was another source of temporal noise prevalent throughout our study period. Incorporating inter-annual variation in our state-space model improved forecasting accuracy, albeit to a lesser extent than adding intra-annual variation. Unlike intra-annual variation, modeled as a continuous variable using date-of-year, we modeled inter-annual variation as a categorical variable with an independent effect for each year. This approach for modeling inter-annual variation makes minimal assumptions about temporal trends but has some costs. Increased model complexity is one cost, as fitting each year separately requires an additional parameter for each year. Our Bayesian approach enabled us to increase our confidence that the year terms represented measurement error, rather than forest regrowth, by incorporating prior information from reference sites with no structural change. In contrast to approaches such as Kennedy et al. (2010) that smooth noise in Landsat time series before fitting trend models, our state-space models propagate uncertainty from inter-annual variability through to model output. A cost of simultaneously estimating both measurement and process error is that state-space models can be more difficult to fit than models that estimate error components in separate steps (Auger-Méthé et al. 2020). A final cost to our approach for modeling inter-annual variability is a limited ability to forecast the effects of inter-annual variation since categorical effects cannot be extrapolated without data. Modeling temporal variation in spectral reflectance as a function of covariates, such as climate (Zhang et al. 2014), topography (Bohlman 2010), or forest type (Pasquarella et al. 2016), has potential to improve our model's forecasting ability. Nevertheless, even without incorporating year effects for forecasted years, the inter-annual model increased forecasting accuracy. This result suggests that accounting for year-to-year variation improved the estimation of our logistic growth process model, leading to more realistic trajectories across the entire time series.

The incorporation of Landsat–lidar fusion into our measurement model enabled us to model canopy height dynamics over time. Modeling canopy height as a state variable, rather than a multispectral vegetation index (NDVI), provides numerous benefits. Most importantly, canopy height has a physical interpretation that can be related to management targets for reforestation projects, including aboveground carbon (Asner et al. 2013, Chazdon et al. 2016). Unlike NDVI, tree canopy height did not approach its biological maximum during our fifteen-year study. While canopy height trajectories exhibited accelerating rates of change that emphasized successional differences, spectral reflectance tended to saturate early in succession across all sites (Fig. 5). The tendency for NDVI to saturate early in succession is a well-known feature of this index (e.g., (Pickell et al. 2016); however, spectral saturation was prevalent across all vegetation indices calculated for our study site, including NBR (Appendix 1: Fig. S1). A practical advantage of modeling canopy height, rather than a vegetation index, was better discrimination of natural regeneration rates between sites, including nearly five orders of magnitude more certainty in site rankings, relative to NDVI models (Fig. 6) and improved agreement between model-derived successional rate and observed percentage tree cover change (Fig. 7). We suggest that this decreased uncertainty reflects the greater biological realism of modeling canopy height rather than NDVI.

We expected to find decreases in forecasting accuracy as a cost of Landsat–lidar fusion, considering the uncertain relationship between our single-date lidar acquisition and 15 yr of Landsat-derived NDVI. Indeed, the average error when NDVI was used to predict canopy height was 4.20 m, suggesting considerable noise even when relating Landsat to lidar during the same year of acquisition. There are an increasing number of methods to predict lidar-derived forest structure from Landsat data, and many are likely to outperform NDVI as a predictor variable (Avitabile et al. 2012, Ota et al. 2014, Ahmed et al. 2015, Caughlin et al. 2016*b*, Matasci et al. 2018). Nevertheless, our canopy height model provided equivalent to better forecasting compared to NDVI-only models, despite uncertainty in Landsat–lidar fusion. By explicitly modeling both process and measurement error, we were able to monitor canopy dynamics, despite temporal variation in Landsat data. While state-space models have been applied to analyze noisy time series for a range of fields, from fisheries science (Aeberhard et al. 2018) to epidemiology (Cauchemez and Ferguson 2008), this modeling approach is not widely used for Earth observation applications. Instead, remote sensing has focused more on minimizing measurement error than on modeling ecological process. Near-term forecasting, such as our 3-yr forecast window, can provide a way to assess process model performance in the face of measurement error (Dietze et al. 2018).

We anticipate that the increasing availability of high quality remotely sensed data will provide new opportunities for state-space modeling across time and space. A time series of lidar data would likely boost our predictive power by resolving a substantial portion of the residual uncertainty in the relationship between satellite spectral reflectance and forest structure. While repeat lidar is not readily available for regions such as Panama, data sets from the upcoming GEDI mission are likely to yield useful estimates of structure in these regions at 25 m resolution (Duncanson et al. 2020). In terms of spectral reflectance, the temporal and spatial quality of the Landsat data record, as well as its free and open status, is hard to match (Wulder et al. 2019). Nevertheless, Sentinel and other higher spectral resolution satellites may provide greater information than using Landsat NDVI alone. Likewise, utilizing radar information in the state-space model may also yield increased predictive power (Qi et al. 2019). Unmanned airborne systems (UAS) have also demonstrated the potential to measure forest structural attributes in reforesting sites via multi-spectral imagery (Zahawi et al. 2015, Jayathunga et al. 2019) and UAS-borne lidar (Almeida et al. 2019*aa*). Our state-space modeling approach could be applied to account for variability in spectral reflectance between sensors, for example, differences in spectral bandwidth between Landsat satellites. In the context of our models, such an approach would require developing the relationship between spectral reflectance and forest structure for each new sensor added. As a greater diversity of remotely sensed data become available, Bayesian methods can provide statistically rigorous means to combine information from different sources into a single model.

Our state-space approach requires a process model to represent the ecological dynamics of secondary succession. We used a relatively simple logistic model for population growth to model successional trajectories with three parameters: initial value, rate of increase, and biological maximum (carrying capacity). Considering that our models converged with a sample size of Landsat pixels (~250 pixels over 15 yr) that represents a minuscule fraction of available satellite data, we anticipate that fitting more sophisticated models for forest dynamics using our approach is possible. For forest succession, accounting for demographic processes that generate spatial structure at landscape scales, including seed dispersal (Acevedo et al. 2012, Caughlin et al. 2016*a*) and negative density dependence (Kellner and Hubbell 2018), is an important next step. Our Landsat–lidar approach could also be used to parameterize forest dynamic models that include canopy height as a state variable, such as the Ecosystem Demography model (Medvigy et al. 2009, Antonarakis et al. 2011) or the Perfect Plasticity Approximation (Purves and Pacala 2008, Caughlin et al. 2016*a*). In a Bayesian context, data from forest inventory plots could contribute informative priors to estimate forest dynamics from satellite imagery (Chave et al. 2019). Our results serve as proof-of-concept that a state-space modeling approach can disentangle rates of forest succession from Landsat time series. While we focused on 10 sites, our methods could be applied for ecological

inference on forest succession at a range of scales, from parcels to ecoregions.

Limits to the complexity of process models fit with Landsat time series will likely be found at the intersection of social and ecological dynamics. In our study area, socioecological dynamics create a diversity of land cover change trajectories, from swidden agriculture to the expansion of agroforestry systems (Tarbox et al. 2018). Across Latin America, the permanence of secondary forest patches depends on land manager decision-making (Schwartz et al. 2017, Reid et al. 2019). Models that attempt to represent all these multi-scale dynamics, from human behavior to tree demography to national economic trends, can become intractably complex (Walker 2008). We anticipate that process models for tree cover change will be most successful when applied to a subset of the landscape undergoing the same type of land cover trajectory. For our models, we digitized high-resolution imagery to identify sites undergoing reforestation. An alternative approach with better scalability would be to use one of an increasing number of automated tools to characterize disturbance using the Landsat record (Kennedy et al. 2012, Watts and Laffan 2014, Vogelmann et al. 2016). State-space models could then provide an opportunity to infer differences in rates of change between pixels undergoing the same type of land cover trajectory.

Given the urgency of climate change, regional-scale coordination is necessary to ensure optimal reforestation outcomes (Brancalion et al. 2019, Busch et al. 2019, Stanturf et al. 2019). Identifying sites that can be restored using natural regeneration will play a critical role in large reforestation plans, with potential to reduce the cost of extensive tree planting (Chazdon and Uriarte 2016, Molin et al. 2018). We have demonstrated an approach to rank successional rates between naturally regenerating sites during early succession, when initial conditions are critical determinants of longer-term forest recovery (Holl et al. 2018). Altogether, our work presents a step towards operationalizing remote sensing for forest landscape restoration.

Acknowledgments

Funding for the social-ecological research was provided by the National Science Foundation under grant #1415297 in the SBE program. The Global Airborne Observatory is made possible by grants and gifts from private foundations, visionary individuals, and Arizona State University. The GAO Panama flights were supported by the Grantham Foundation for the Protection of the Environment. Juan Requena, Andrii Zaiats, Anand Roopsind, and Cara Applestein provided valuable feedback on a draft of the manuscript.

Literature Cited

Acevedo, M. A., M. Marcano, and R. J. Fletcher Jr. 2012. A diffusive logistic growth model to describe forest recovery. Ecological Modelling 244:13–19.

Aeberhard, W. H., J. Mills Flemming, and A. Nielsen. 2018. Review of state-space models for fisheries science. Annual Review of Statistics and Its Application 5:215–235.

Ahmed, O. S., S. E. Franklin, M. A. Wulder, and J. C. White. 2015. Characterizing stand-level forest canopy cover and height using landsat time series, samples of airborne LiDAR, and the random forest algorithm. ISPRS Journal of Photogrammetry and Remote Sensing 101:89–101.

Aide, T. M., M. L. Clark, H. R. Grau, D. López-Carr, M. A. Levy, D. Redo, M. Bonilla-Moheno, G. Riner, M. J. Andrade-Núñez, and M. Muñiz. 2013. Deforestation and reforestation of Latin America and the Caribbean (2001–2010). Biotropica 45:262–271.

Almeida, D. R. A. et al. 2019*a*. Monitoring the structure of forest restoration plantations with a drone-lidar system. International Journal of Applied Earth Observation and Geoinformation 79:192–198.

Almeida, D. R. A. et al. 2019*b*. The effectiveness of lidar remote sensing for monitoring forest cover attributes and landscape restoration. Forest Ecology and Management 438:34–43.

Antonarakis, A. S., S. S. Saatchi, R. L. Chazdon, and P. R. Moorcroft. 2011. Using Lidar and Radar measurements to constrain predictions of forest ecosystem structure and function. Ecological Applications 21:1120–1137.

Asner, G. P., J. Mascaro, C. Anderson, D. E. Knapp, R. E. Martin, T. Kennedy-Bowdoin, M. van Breugel, S. Davies, J. S. Hall, and H. C. Muller-Landau. 2013. High-fidelity national carbon mapping for resource management and REDD+. Carbon Balance and Management 8:7.

Auger-Méthé, M. et al. 2020. An introduction to state-space modeling of ecological time series. arXiv:2002.02001 [q-bio, stat].

Avitabile, V., A. Baccini, M. A. Friedl, and C. Schmullius. 2012. Capabilities and limitations of Landsat and land cover data for aboveground woody biomass estimation of Uganda. Remote Sensing of Environment 117:366–380.

Bernardis, C. G. D., F. Vicente-Guijalba, T. Martinez-Marin, and J. M. Lopez-Sanchez. 2015. Particle filter approach for crop phenological stage estimation using time series of NDVI images. Pages 3385–3388 *in* 2015 IEEE International Geoscience and Remote Sensing Symposium (IGARSS). Milan, Italy.

Betancourt, M. 2017. A Conceptual Introduction to Hamiltonian Monte Carlo. arXiv:1701.02434 [stat].

Bohlman, S. A. 2010. Landscape patterns and environmental controls of deciduousness in forests of central Panama. Global Ecology and Biogeography 19:376–385.

Bolton, D. K., J. C. White, M. A. Wulder, N. C. Coops, T. Hermosilla, and X. Yuan. 2018. Updating stand-level forest inventories using airborne laser scanning and Landsat time series data. International Journal of Applied Earth Observation and Geoinformation 66:174–183.

Brancalion, P. H. S. et al. 2019. Global restoration opportunities in tropical rainforest landscapes. Science Advances 5: eaav3223.

Busch, J., J. Engelmann, S. C. Cook-Patton, B. W. Griscom, T. Kroeger, H. Possingham, and P. Shyamsundar. 2019. Potential for low-cost carbon dioxide removal through tropical reforestation. Nature Climate Change 9:463.

Cauchemez, S., and N. M. Ferguson. 2008. Likelihood-based estimation of continuous-time epidemic models from time-series data: application to measles transmission in London. Journal of the Royal Society Interface 5:885–897.

Caughlin, T. T., M. de la Peña-Domene, and C. Martínez-Garza. 2019. Demographic costs and benefits of natural regeneration during tropical forest restoration. Ecology Letters 22:34–44.

Caughlin, T. T., S. Elliott, and J. W. Lichstein. 2016*a*. When does seed limitation matter for scaling up reforestation from patches to landscapes? Ecological Applications 26:2437–2448.

Caughlin, T. T., S. W. Rifai, S. J. Graves, G. P. Asner, and S. A. Bohlman. 2016*b*. Integrating LiDAR-derived tree height and Landsat satellite reflectance to estimate forest regrowth in a tropical agricultural landscape. Remote Sensing in Ecology and Conservation 2:190–203.

Caughlin, T. T., and C. H. Wilson. 2020. GitHub Repository trevorcaughlin/StateSpaceLandsat/tree/v1.0. https://doi.org/10.5281/zenodo.3873639

Chave, J. et al. 2019. Ground data are essential for biomass remote sensing missions. Surveys in Geophysics 40:863–880.

Chazdon, R. L. 2014. Second growth: The promise of tropical forest regeneration in an age of deforestation. University of Chicago Press, Chicago, Illinois, USA.

Chazdon, R. L. et al. 2016. Carbon sequestration potential of second-growth forest regeneration in the Latin American tropics. Science Advances 2:e1501639.

Chazdon, R. L., and M. Uriarte. 2016. Natural regeneration in the context of large-scale forest and landscape restoration in the tropics. Biotropica 48:709–715.

Chen, D., T. V. Loboda, A. Krylov, and P. V. Potapov. 2016. Mapping stand age dynamics of the Siberian larch forests from recent Landsat observations. Remote Sensing of Environment 187:320–331.

Clark, J. S., and O. N. Bjørnstad. 2004. Population time series: process variability, observation errors, missing values, lags, and hidden states. Ecology 85:3140–3150.

Coops, N. C., S. N. Gillanders, M. A. Wulder, S. E. Gergel, T. Nelson, and N. R. Goodwin. 2010. Assessing changes in forest fragmentation following infestation using time series Landsat imagery. Forest Ecology and Management 259:2355–2365.

Coops, N. C., and M. A. Wulder. 2019. Breaking the habit(at). Trends in Ecology & Evolution 34:585–587.

Dennis, B., and J. M. Ponciano. 2014. Density-dependent state-space model for population-abundance data with unequal time intervals. Ecology 95:2069–2076.

Dietze, M. C. et al. 2018. Iterative near-term ecological forecasting: Needs, opportunities, and challenges. Proceedings of the National Academy of Sciences USA 115:1424–1432.

Dorazio, R. M., J. A. Royle, B. Söderström, and A. Glimskär. 2006. Estimating species richness and accumulation by modeling species occurrence and detectability. Ecology 87:842–854.

Duncanson, L., A. Neuenschwander, S. Hancock, N. Thomas, T. Fatoyinbo, M. Simard, C. A. Silva, J. Armston, S. B. Luthcke, M. Hofton, J. R. Kellner and R. Dubayah. 2020. Biomass estimation from simulated GEDI, ICESat-2 and NISAR across environmental gradients in Sonoma County, California. Remote Sensing of Environment 242:111779.

Dutrieux, L. P., C. C. Jakovac, S. H. Latifah, and L. Kooistra. 2016. Reconstructing land use history from Landsat time-series: Case study of a swidden agriculture system in Brazil. International Journal of Applied Earth Observation and Geoinformation 47:112–124.

Evans, K., M. R. Guariguata, and P. H. S. Brancalion. 2018. Participatory monitoring to connect local and global priorities for forest restoration. Conservation Biology 32:525–534.

Estrada-Villegas, S., M. Bailón, J. S. Hall, S. A. Schnitzer, B. L. Turner, T. Caughlin, and M. van Breugel. 2020. Edaphic factors and initial conditions influence successional trajectories of early regenerating tropical dry forests. Journal of Ecology 108:160–174.

Frazier, R. J., N. C. Coops, M. A. Wulder, T. Hermosilla, and J. C. White. 2018. Analyzing spatial and temporal variability in short-term rates of post-fire vegetation return from Landsat time series. Remote Sensing of Environment 205:32–45.

Frolking, S., M. W. Palace, D. B. Clark, J. Q. Chambers, H. H. Shugart, and G. C. Hurtt. 2009. Forest disturbance and recovery: a general review in the context of spaceborne remote sensing of impacts on aboveground biomass and canopy structure. Journal of Geophysical Research Biogeosciences 114:1–27.

Goodrich, B., J. Gabry, I. Ali, and S. Brilleman. 2020. rstanarm: Bayesian applied regression modeling via Stan. R package version 2.21.1, https://mc-stan.org/rstanarm

Graves, S. J., T. T. Caughlin, G. P. Asner, and S. A. Bohlman. 2018. A tree-based approach to biomass estimation from remote sensing data in a tropical agricultural landscape. Remote Sensing of Environment 218:32–43.

Griscom, B. W. et al. 2017. Natural climate solutions. Proceedings of the National Academy of Sciences USA 114:11645–11650.

Heckadon-Moreno, S. H. 2009. De selvas a potreros: la colonización santeña en Panamá, 1850–1980. Exedra Books, Panama City, Panama.

Hermosilla, T., M. A. Wulder, J. C. White, N. C. Coops, and G. W. Hobart. 2015. An integrated Landsat time series protocol for change detection and generation of annual gap-free surface reflectance composites. Remote Sensing of Environment 158:220–234.

Holl, K. D., and T. M. Aide. 2011. When and where to actively restore ecosystems? Forest Ecology and Management 261:1558–1563.

Holl, K. D., J. L. Reid, F. Oviedo-Brenes, A. J. Kulikowski, and R. A. Zahawi. 2018. Rules of thumb for predicting tropical forest recovery. Applied Vegetation Science 21:669–677.

Hooten, M. B., C. K. Wikle, R. M. Dorazio, and J. A. Royle. 2007. Hierarchical spatiotemporal matrix models for characterizing invasions. Biometrics 63:558–567.

Jayathunga, S., T. Owari, and S. Tsuyuki. 2019. Digital aerial photogrammetry for uneven-aged forest management: assessing the potential to reconstruct canopy structure and estimate living biomass. Remote Sensing 11:338.

Kellner, J. R., and S. P. Hubbell. 2017. Adult mortality in a low-density tree population using high-resolution remote sensing. Ecology 98:1700–1709.

Kellner, J. R., and S. P. Hubbell. 2018. Density-dependent adult recruitment in a low-density tropical tree. Proceedings of the National Academy of Sciences USA 115:11268–11273.

Kennedy, R. E., Z. Yang, and W. B. Cohen. 2010. Detecting trends in forest disturbance and recovery using yearly Landsat time series: 1. LandTrendr—Temporal segmentation algorithms. Remote Sensing of Environment 114:2897–2910.

Kennedy, R. E., Z. Yang, W. B. Cohen, E. Pfaff, J. Braaten, and P. Nelson. 2012. Spatial and temporal patterns of forest disturbance and regrowth within the area of the Northwest Forest Plan. Remote Sensing of Environment 122:117–133.

Lee, J., J. Im, K. Kim, and L. Quackenbush. 2018. Machine learning approaches for estimating forest stand height using plot-based observations and airborne LiDAR data. Forests 9:268.

Mansourian, S., and D. Vallauri. 2014. Restoring forest landscapes: Important lessons learnt. Environmental Management 53:241–251.

Marvin, D. C., G. P. Asner, D. E. Knapp, C. B. Anderson, R. E. Martin, F. Sinca, and R. Tupayachi. 2014. Amazonian landscapes and the bias in field studies of forest structure and biomass. Proceedings of the National Academy of Sciences USA 111:E5224–E5232.

Masek, J. G., E. F. Vermote, N. E. Saleous, R. Wolfe, F. G. Hall, K. F. Huemmrich, F. Gao, J. Kutler, and T.-K. Lim. 2006. A Landsat surface reflectance dataset for North America, 1990-2000. IEEE Geoscience and Remote Sensing Letters 3:68–72.

Matasci, G., T. Hermosilla, M. A. Wulder, J. C. White, N. C. Coops, G. W. Hobart, D. K. Bolton, P. Tompalski, and C. W. Bater. 2018. Three decades of forest structural dynamics over Canada's forested ecosystems using Landsat time-series and lidar plots. Remote Sensing of Environment 216:697–714.

Medvigy, D., S. C. Wofsy, J. W. Munger, D. Y. Hollinger, and P. R. Moorcroft. 2009. Mechanistic scaling of ecosystem function and dynamics in space and time: Ecosystem Demography model version 2. Journal of Geophysical Research Biogeosciences 114:1–21.

Misra, G., A. Buras, M. Heurich, S. Asam, and A. Menzel. 2018. LiDAR derived topography and forest stand characteristics largely explain the spatial variability observed in MODIS land surface phenology. Remote Sensing of Environment 218:231–244.

Molin, P. G., R. Chazdon, S. F. B. Ferraz, and P. H. S. Brancalion. 2018. A landscape approach for cost-effective large-scale forest restoration. Journal of Applied Ecology 55:2767–2778.

Montenegro, C., and M. Branco. 2016. Bayesian state-space approach to biomass dynamic models with skewed and heavy-tailed error distributions. Fisheries Research 181:48–62.

Nathan, H. W., M. N. Clout, J. W. B. MacKay, E. C. Murphy, and J. C. Russell. 2015. Experimental island invasion of house mice. Population Ecology 57:363–371.

Nguyen, T. H., S. D. Jones, M. Soto-Berelov, A. Haywood, and S. Hislop. 2018. A spatial and temporal analysis of forest dynamics using Landsat time-series. Remote Sensing of Environment 217:461–475.

Norden, N. et al. 2015. Successional dynamics in Neotropical forests are as uncertain as they are predictable. Proceedings of the National Academy of Sciences USA 112:8013–8018.

Ota, T. et al. 2014. Estimation of airborne Lidar-derived tropical forest canopy height using Landsat time series in Cambodia. Remote Sensing 6:10750–10772.

Pasquarella, V. J., C. E. Holden, L. Kaufman, and C. E. Woodcock. 2016. From imagery to ecology: leveraging time series of all available Landsat observations to map and monitor ecosystem state and dynamics. Remote Sensing in Ecology and Conservation 2:152–170.

Pettorelli, N., J. O. Vik, A. Mysterud, J.-M. Gaillard, C. J. Tucker, and N. Chr. Stenseth. 2005. Using the satellite-derived NDVI to assess ecological responses to environmental change. Trends in Ecology & Evolution 20:503–510.

Pflugmacher, D., W. B. Cohen, R. E. Kennedy, and Z. Yang. 2014. Using Landsat-derived disturbance and recovery history and lidar to map forest biomass dynamics. Remote Sensing of Environment 151:124–137.

Pickell, P. D., T. Hermosilla, R. J. Frazier, N. C. Coops, and M. A. Wulder. 2016. Forest recovery trends derived from Landsat time series for North American boreal forests. International Journal of Remote Sensing 37:138–149.

Plummer, M. 2015. Cuts in Bayesian graphical models. Statistics and Computing 25:37–43.

Poorter, L. et al. 2016. Biomass resilience of Neotropical secondary forests. Nature 530:211–214.

Pugh, T. A. M., M. Lindeskog, B. Smith, B. Poulter, A. Arneth, V. Haverd, and L. Calle. 2019. Role of forest regrowth in global carbon sink dynamics. Proceedings of the National Academy of Sciences USA 116:4382–4387.

Purves, D., and S. Pacala. 2008. Predictive models of forest dynamics. Science 320:1452–1453.

Qi, W., S.-K. Lee, S. Hancock, S. Luthcke, H. Tang, J. Armston, and R. Dubayah. 2019. Improved forest height estimation by fusion of simulated GEDI Lidar data and TanDEM-X InSAR data. Remote Sensing of Environment 221:621–634.

Reed, B. C., J. F. Brown, D. VanderZee, T. R. Loveland, J. W. Merchant, and D. O. Ohlen. 1994. Measuring phenological variability from satellite imagery. Journal of Vegetation Science 5:703–714.

Reid, J. L., M. E. Fagan, J. Lucas, J. Slaughter, and R. A. Zahawi. 2019. The ephemerality of secondary forests in southern Costa Rica. Conservation Letters 12:e12607.

Requena-Mullor, J. M., A. Reyes, P. Escribano, and J. Cabello. 2018. Assessment of ecosystem functioning from space: Advancements in the habitats directive implementation. Ecological Indicators 89:893–902.

Richit, L. A., C. Bonatto, R. V. da Silva, and J. M. V. Grzybowski. 2019. Prognostics of forest recovery with r.recovery GRASS-GIS module: an open-source forest growth simulation model based on the diffusive-logistic equation. Environmental Modelling & Software 111:108–120.

Roberts, D. R. et al. 2017. Cross-validation strategies for data with temporal, spatial, hierarchical, or phylogenetic structure. Ecography 40:913–929.

Royle, J. A., J. D. Nichols, K. U. Karanth, and A. M. Gopalaswamy. 2009. A hierarchical model for estimating density in camera-trap studies. Journal of Applied Ecology 46:118–127.

Rudel, T. K. 2012. The human ecology of regrowth in the tropics. Journal of Sustainable Forestry 31:340–354.

Schmidt, J. H., C. L. McIntyre, and M. C. MacCluskie. 2013. Accounting for incomplete detection: What are we estimating and how might it affect long-term passerine monitoring programs? Biological Conservation 160:130–139.

Schroeder, T. A., M. A. Wulder, S. P. Healey, and G. G. Moisen. 2011. Mapping wildfire and clearcut harvest disturbances in boreal forests with Landsat time series data. Remote Sensing of Environment 115:1421–1433.

Schwartz, N. B., M. Uriarte, R. DeFries, V. H. Gutierrez-Velez, and M. A. Pinedo-Vasquez. 2017. Land-use dynamics influence estimates of carbon sequestration potential in tropical second-growth forest. Environmental Research Letters 12:074023.

Senf, C., D. Pflugmacher, M. Heurich, and T. Krueger. 2017. A Bayesian hierarchical model for estimating spatial and temporal variation in vegetation phenology from Landsat time series. Remote Sensing of Environment 194:155–160.

Shoo, L. P., K. Freebody, J. Kanowski, and C. P. Catterall. 2016. Slow recovery of tropical old-field rainforest regrowth and the value and limitations of active restoration. Conservation Biology 30:121–132.

Sloan, S. 2015. The development-driven forest transition and its utility for REDD+. Ecological Economics 116:1–11.

Song, C., C. E. Woodcock, and X. Li. 2002. The spectral/temporal manifestation of forest succession in optical imagery: the potential of multitemporal imagery. Remote Sensing of Environment 82:285–302.

Song, C., C. E. Woodcock, K. C. Seto, M. P. Lenney, and S. A. Macomber. 2001. Classification and change detection using Landsat TM data: When and how to correct atmospheric effects? Remote Sensing of Environment 75:230–244.

Stan Development Team. 2016. Stan modeling language: User's guide and reference manual. Version.

Stanturf, J. A., M. Kleine, S. Mansourian, J. Parrotta, P. Madsen, P. Kant, J. Burns, and A. Bolte. 2019. Implementing forest landscape restoration under the Bonn Challenge: a systematic approach. Annals of Forest Science 76:50.

Tarbox, B. C., C. Fiestas, and T. T. Caughlin. 2018. Divergent rates of change between tree cover types in a tropical pastoral region. Landscape Ecology 33:2153–2167.

Tarbox, B. C., C. Fiestas, and T. T. Caughlin. 2019. Data from: Divergent rates of change between tree cover types in a tropical pastoral region. Dryad, Data set. https://doi.org/10.5061/dryad.q5r472k

Tsoularis, A., and J. Wallace. 2002. Analysis of logistic growth models. Mathematical Biosciences 179:21–55.

Ver Planck, N. R., A. O. Finley, J. A. Kershaw, A. R. Weiskittel, and M. C. Kress. 2018. Hierarchical Bayesian models for small area estimation of forest variables using LiDAR. Remote Sensing of Environment 204:287–295.

Verbesselt, J., R. Hyndman, G. Newnham, and D. Culvenor. 2010. Detecting trend and seasonal changes in satellite image time series. Remote Sensing of Environment 114:106–115.

Vogelmann, J. E., A. L. Gallant, H. Shi, and Z. Zhu. 2016. Perspectives on monitoring gradual change across the continuity of Landsat sensors using time-series data. Remote Sensing of Environment 185:258–270.

Walker, R. 2008. Forest transition: Without complexity, without scale. Professional Geographer 60:136–140.

Watts, L. M., and S. W. Laffan. 2014. Effectiveness of the BFAST algorithm for detecting vegetation response patterns in a semi-arid region. Remote Sensing of Environment 154:234–245.

White, J. C., M. A. Wulder, T. Hermosilla, and N. C. Coops. 2019. Satellite time series can guide forest restoration. Nature 569:630.

White, J. C., M. A. Wulder, T. Hermosilla, N. C. Coops, and G. W. Hobart. 2017. A nationwide annual characterization of 25 years of forest disturbance and recovery for Canada using Landsat time series. Remote Sensing of Environment 194:303–321.

Wright, S. J., and M. J. Samaniego. 2008. Historical, demographic, and economic correlates of land-use change in the Republic of Panama. Ecology and Society 13:17.

Wulder, M. A., J. C. White, S. N. Goward, J. G. Masek, J. R. Irons, M. Herold, W. B. Cohen, T. R. Loveland, and C. E. Woodcock. 2008. Landsat continuity: Issues and opportunities for land cover monitoring. Remote Sensing of Environment 112:955–969.

Wulder, M. A., et al. 2019. Current status of Landsat program, science, and applications. Remote Sensing of Environment 225:127–147.

Zahawi, R. A., J. P. Dandois, K. D. Holl, D. Nadwodny, J. L. Reid, and E. C. Ellis. 2015. Using lightweight unmanned aerial vehicles to monitor tropical forest recovery. Biological Conservation 186:287–295.

Zeileis, A., F. Cribari-Neto, B. Gruen, I. Kosmidis. 2018. betareg: Beta regression. https://cran.r-project.org/web/packages/betareg/

Zelnik, Y. R., J.-F. Arnoldi, and M. Loreau. 2019. The three regimes of spatial recovery. Ecology 100:e02586.

Zhang, X., B. Tan, and Y. Yu. 2014. Interannual variations and trends in global land surface phenology derived from enhanced vegetation index during 1982–2010. International Journal of Biometeorology 58:547–564.

Zhu, Z. et al. 2019. Benefits of the free and open Landsat data policy. Remote Sensing of Environment 224:382–385.

Zhu, Z., C. E. Woodcock, and P. Olofsson. 2012. Continuous monitoring of forest disturbance using all available Landsat imagery. Remote Sensing of Environment 122:75–91.

Supporting Information

Additional supporting information may be found online at: http://onlinelibrary.wiley.com/doi/10.1002/eap.2208/full

Data Availability

Landsat data is publicly available via USGS Earth Explorer (see Methods: Landsat data). *The digitized tree data used for validation is available on Dryad (Tarbox et al. 2019). Stan code to run state-space models is archived with Zenodo: http://doi.org/10.5281/zenodo.3873639*